Article

Stochastic Liouville Equations for Coherent Multidimensional Spectroscopy of Excitons

Frantis#ek S#anda, and Shaul Mukamel

More About This Article

Additional resources and features associated with this article are available within the HTML version:

- Supporting Information
- Access to high resolution figures
- Links to articles and content related to this article
- Copyright permission to reproduce figures and/or text from this article

View the Full Text HTML

Stochastic Liouville Equations for Coherent Multidimensional Spectroscopy of Excitons

František Šanda*,†ᵈ and Shaul Mukamel‡

*Faculty of Mathematics and Physics, Institute of Physics, Charles University, Ke Karlovu 5,
Prague, 121 16 Czech Republic, and Department of Chemistry, University of California,
Irvine, California 92697-2025*

Signatures of chemical exchange and spectral diffusion in 2D photon-echo line shapes of molecular aggregates are studied using model calculations for a dimer whose Hamiltonian parameters are stochastically modulated. Cross peaks induced by chemical exchange and by exciton transport have different dynamics and distinguish two models which have the same absorption spectrum (a two-state jump bath modulation model of a dimer and a four-state jump bath model of a single chromophore). Slow Gaussian−Markovian spectral diffusion of a symmetric dimer induces new peaks which are damped as the dipole moment is equilibrated. These effects require an explicit treatment of the bath and may not be described by lower-level theories such as the Redfield equations, which eliminate the bath.

1. Introduction

Exciton models are widely used in the description of the coherent nonlinear optical response of complex systems.[1] Vibrational spectra of proteins[2−6] and liquid water[7] and electronic spectra of photosynthetic antenae[8] are a few examples. Bath-induced fluctuations of transition frequencies and couplings affect the electronic and transport properties of aggregates (e.g., photosynthetic antenae).

A broad arsenal of techniques has been developed toward the simulation of two-dimensional coherent spectroscopy (2DCS) signals.[1] Direct simulation of the optical response requires repeated diagonalizations of the system Hamiltonian at many time points. The response is then given by a path integral over the trajectories of the time-dependent eigenvalues and the overlap factors of the instantaneous eigenstates at different times.[9,10]

The fluctuating time-dependent Hamiltonian $H(t)$ defines the instantaneous (adiabatic) basis $|\varphi_j(t)\rangle$ and energies $\varepsilon_j(t)$ (we set $\hbar = 1$)

$$H(t)|\varphi_j(t)\rangle = \varepsilon_j(t)|\varphi_j(t)\rangle$$

Direct evaluation of the time evolution operator, when the time t is divided into $N \rightarrow \infty$ short segments $\Delta t \equiv t/N$ gives

$$\mathcal{U} \equiv T \exp\left[-i\int_0^t d\tau H(\tau)\right] = T\prod_{n=1}^{N} \exp[-iH(t_n)\Delta t]$$

$$t_n = n\Delta t \quad (1)$$

where T is time ordering operator. By adopting the matrix representation $\mathcal{U}_{jk} \equiv \langle\varphi_j(t)|\mathcal{U}\varphi_k(0)\rangle$, we get

$$\tilde{\mathcal{U}} = T\prod_{n=1}^{N} U_n S_n \quad (2)$$

Here

$$(U_n)_{jj'} = \exp[-i\varepsilon_j(t_n)\Delta t]\delta_{jj'}$$

is the adiabatic propagator, and the nonadiabatic coupling matrix

$$(S_n)_{jj'} = \langle\varphi_j(t_n)|\varphi_{j'}(t_{n-1})\rangle$$

represents the overlap of the adiabatic states at two adjacent points.

Implementing eq 1 is numerically expensive. Moreover, one must typically account for various fluctuation scenarios and average over sufficiently long trajectories (or, equivalently by ergodic hypothesis, over possible paths) of the fluctuating Hamiltonian.

More affordable simulations are feasible when the fluctuations are small and fast. The response can then be calculated by sums over delocalized eigenstates of the average Hamiltonian, where dephasing rates are introduced phenomenologically.[11] Exciton transport may be accounted for by using the Redfield equations[1,12,13] for the reduced Liouville space dynamics of the chromophores. A quasiparticle approach based on the nonlinear exciton equations allows the interpretation of signals in terms of exciton scattering.[1] Very slow fluctuations can be readily incorporated by static averaging of the signals over their realizations.[14]

The stochastic Liouville equations (SLE)[15−17] allow the modeling of strong fluctuations with arbitrary time scales, provided they can be described by a few classical collective coordinates which satisfy a Markovian master equation. The path integrals of eq 2 and the final averaging are avoided by
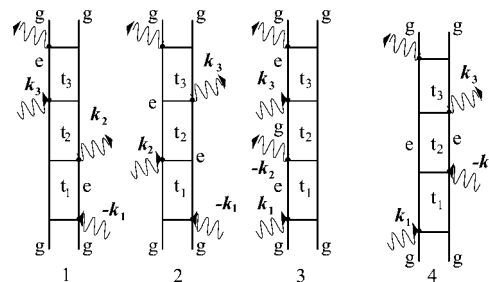

Figure 1. Double-sided Feynman diagrams for the Liouville space pathways contributing to the third-order response in the phase-matching direction $\mathbf{k_I} = -\mathbf{k_1} + \mathbf{k_2} + \mathbf{k_3}$ and $\mathbf{k_{II}} = \mathbf{k_1} - \mathbf{k_2} + \mathbf{k_3}$ (eq 7).

 * To whom correspondence should be addressed. E-mail: sanda@karlov.mff.cuni.cz (F.Š.); smukamel@uci.edu (S.M.).
 † Charles University.
 ‡ University of California.

Coherent Multidimensional Spectroscopy of Excitons
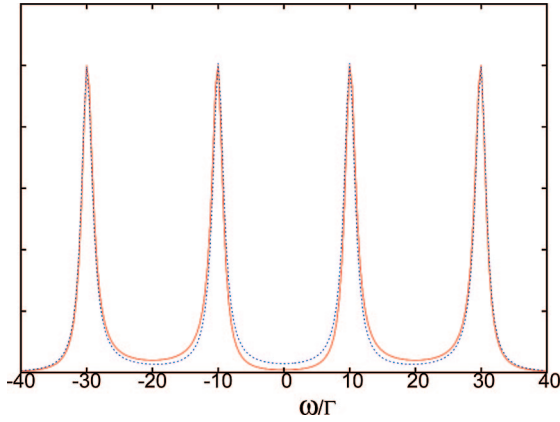
J. Phys. Chem. B, Vol. 112, No. 45, 2008 **14213**

Figure 2. Absorption line shapes (eq 6) of a dimer with two-state bath fluctuations (eqs 3 and 4) (solid line) and a monomer with four-state bath fluctuations (eqs 18 and 19) (dotted line) in the static limit. The dimer peaks correspond to resonance with (from left to right) ε_{2u}, ε_{2d}, ε_{1d}, ε_{1u} levels. Parameters: Dimer: $\varepsilon_{1u} = 30\Gamma$, $\varepsilon_{1d} = 10\Gamma$, $\varepsilon_{2u} = -30\Gamma$, $\varepsilon_{2d} = -10\Gamma$, $J_u = J_d = 0$, $k_u = k_d = k = \Gamma$. Monomer: $\varepsilon_1 = 30\Gamma$, $\varepsilon_2 = 10\Gamma$, $\varepsilon_3 = -30\Gamma$, $\varepsilon_4 = -10\Gamma$, $k_{12}k_{21} = k_{13} = k_{31} = k_{14} = k_{41} = k_{23} = k_{32} = k_{24} = k_{42} = k_{34} = k_{43} = \Gamma/3$, $\mu_{4sj} = \sqrt{2}\,\mu_{dim}$. All the lineshapes shown at Figures 28 are calculated by solving the full SLE model, and not by using the various limiting approximations discussed in the main text.

calculating the density distributions in the joint system + bath space. The SLE generalize the Redfield equations, which are limited to fast fluctuations where the bath degrees of freedom can be eliminated. We have recently applied the SLE to calculate 2D line shapes of a single chromophore whose transition frequency undergoes a stochastic modulation due to hydrogen bonding in water[18,19] or organic solvents.[20,21] Excitonic spectra of a multichromophoric system (trialanine) were described by the SLE approach for a limited class of models and delay times.[10]

In this paper, we apply the SLE to a model dimer interacting with a classical bath. We predict the complete delay time evolution of 2D signals and show new effects of interchromophore coupling, as well as spectral diffusion characteristics of the finite fluctuation time. Two types of stochastic models are considered; discrete chemical exchange will be described by a two-state jump model for the bath, and continuous spectral diffusion will account for using a Gaussian−Markovian coordinate (high-temperature limit of a Brownian overdamped oscillator). We show how the 2D signals may distinguish the model from a nonexcitonic system which has the same linear response. Some effects which are missed in the simpler Redfield treatment are pointed out.

2. Stochastic Liouville Equations for the Molecular Dimer

We consider a dimer with two one-exciton states, $|e_1\rangle = B_1^\dagger|g\rangle$ and $|e_2\rangle = B_2^\dagger|g\rangle$, and one doubly excited state, $|f_1\rangle \equiv B_1^\dagger B_2^\dagger|g\rangle$, described by the Frenkel-exciton Hamiltonian[1,22−24]

$$H = \varepsilon_1(t)B_1^\dagger B_1 + \varepsilon_2(t)B_2^\dagger B_2 + J(t)(B_2^\dagger B_1 + B_1^\dagger B_2) +$$
$$\Delta B_1^\dagger B_2^\dagger B_1 B_2 \quad (3)$$

Both the coupling J and energies ϵ_j undergo stochastic fluctuations. We will assume that the doubly excited state is strongly shifted, $\Delta \rightarrow \infty$, so that it does not contribute to the optical signals near the single-exciton frequency $\omega \approx \varepsilon$.

A discrete fluctuation model is introduced by an additional bath degree of freedom with two states u (up) and d (down), representing, for example, two conformers of the molecule or solvent configurations. We assume that the Hamiltonian parameters jump stochastically between two values J_u, ε_{1u}, ε_{2u} and J_d, ε_{1d}, ε_{2d} corresponding to the two configurations. The transitions between these states are described by a Markovian Pauli master equation[25] with down (k_d) and up (k_u) jump rates, respectively.

$$\left(\frac{d\rho_u}{dt}\right)_M = -k_d\rho_u + k_u\rho_d$$
$$\left(\frac{d\rho_d}{dt}\right)_M = k_d\rho_u - k_u\rho_d \quad (4)$$

The entire density matrix, defined in the joint system + bath space, is described by the stochastic Liouville equation[15,16]

$$\frac{d\rho}{dt} = -i[H, \rho] + \left(\frac{d\rho}{dt}\right)_M \equiv \mathcal{L}\rho$$

Here, ρ carries three indices representing bra and ket variables of the system Liouville space and one index denoting the state of the bath.

Since the Hamiltonian (eq 3) conserves the number of excitons, the Liouville operator $\mathcal{L}$ is block-diagonal, with separate blocks corresponding to the gg, ee, ge, and eg manifolds. We define the basis set for ground-state evolution ($|gg; u\rangle\rangle$, $|gg; d\rangle\rangle$), with the block

$$\mathcal{L}_{gg,gg} = \begin{pmatrix} -k_d & k_u \\ k_d & -k_u \end{pmatrix}$$

The coherence (eg) evolution is described in the following basis set $|e_1g; u\rangle\rangle$, $|e_1g; d\rangle\rangle$, $|e_2g; u\rangle\rangle$, and $|e_2g; d\rangle\rangle$ by the Liouvillean

$$\mathcal{L}_{eg,eg} = \begin{pmatrix} -k_d - i\varepsilon_{1u} & k_u & -iJ_u & 0 \\ k_d & -k_u - i\varepsilon_{1d} & 0 & -iJ_d \\ -iJ_u & 0 & -k_d - i\varepsilon_{2u} & k_u \\ 0 & -iJ_d & k_d & -k_u - i\varepsilon_{2d} \end{pmatrix}$$

Finally, the excited-state block $|e_1e_1; u\rangle\rangle$, $|e_1e_1; d\rangle\rangle$, $|e_1e_2; u\rangle\rangle$, $|e_1e_2; d\rangle\rangle$, $|e_2e_1; u\rangle\rangle$, $|e_2e_1; d\rangle\rangle$, $|e_2e_2; u\rangle\rangle$, $|e_2e_2; d\rangle\rangle$ is represented by

$$\mathcal{L}_{ee',ee'} =$$
$$\begin{pmatrix}
-k_d & k_u & iJ_u & 0 & -iJ_u & 0 & 0 & 0 \\
k_d & -k_u & 0 & iJ_d & 0 & -iJ_d & 0 & 0 \\
iJ_u & 0 & -k_d - i\Delta\varepsilon_u & k_u & 0 & 0 & -iJ_u & 0 \\
0 & iJ_d & k_d & -k_u - i\Delta\varepsilon_d & 0 & 0 & 0 & -iJ_d \\
-iJ_u & 0 & 0 & 0 & -k_d + i\Delta\varepsilon_u & k_u & iJ_u & 0 \\
0 & -iJ_d & 0 & 0 & k_d & -k_u + i\Delta\varepsilon_d & 0 & iJ_d \\
0 & 0 & -iJ_u & 0 & iJ_u & 0 & -k_d & k_u \\
0 & 0 & 0 & -iJ_d & 0 & iJ_d & k_d & -k_u
\end{pmatrix}$$

where we have denoted $\Delta\varepsilon_d \equiv \varepsilon_{1d} - \varepsilon_{2d}$, $\Delta\varepsilon_u \equiv \varepsilon_{1u} - \varepsilon_{2u}$. With $\mathcal{L}_{ge,ge} = \mathcal{L}^*_{eg,eg}$, the description is complete.

The Green's function solution of the Liouville equation is

$$\mathcal{G}(t) \equiv \theta(t)\exp\mathcal{L}t$$

In the frequency domain, $\mathcal{G}(\omega) = \int_0^\infty e^{i\omega t}\mathcal{G}(t)dt$, we have

$$\mathcal{G}(\omega) = -[i\omega + \mathcal{L}]^{-1} \quad (5)$$

Like $\mathcal{L}$, the Green's function is block-diagonal as well. For instance, the time domain Green's function for the gg block reads

$$\mathcal{G}_{gg,gg}(t) = \frac{1}{k_d + k_u}\begin{pmatrix} k_u & k_u \\ k_d & k_d \end{pmatrix} + \frac{e^{-(k_d+k_u)t}}{k_d+k_u}\begin{pmatrix} k_d & -k_u \\ -k_d & k_u \end{pmatrix}$$

In the other manifolds, the time domain Green's functions will be calculated numerically by spectral decomposition of the Liouville operator. In the frequency domain, all of the block matrix inversions (eq 5) can be performed analytically in closed, though somewhat lengthy, form.

Averaging over the bath variable is made with respect to the equilibrium bath density

$$|\rho^{(exp)}\rangle = \frac{1}{k_d + k_u}\begin{pmatrix} k_u \\ k_d \end{pmatrix}$$

and the summation over final states is represented by the scalar product with the vector $\langle I| = (1, 1)$.

3. The Two-Dimensional Signals

We shall calculate the response of the system to three laser pulses. The interaction is given by $H_{int} = -E(t)D_{int}$, where

$$D_{int} = [\mu_1(B_1^\dagger + B_1) + \mu_2(B_2^\dagger + B_2)]$$

is the dipole operator. We consider impulsive experiments performed with short laser pulses. The linear response function is

$$S(t_1) = i\langle\langle\mu|\mathcal{G}(t_1)\mu^{(-)}|\rho(0)\rangle\rangle$$

and the third-order response function[26]

$$S(t_3, t_2, t_1) = i^3\langle\langle\mu|\mathcal{G}(t_3)\mu^{(-)}\mathcal{G}(t_2)\mu^{(-)}\mathcal{G}(t_1)\mu^{(-)}|\rho(0)\rangle\rangle$$

where $\mu^{(-)} \equiv [D_{int},...]$ is the dipole superoperator and $\langle\langle\mu|... = \langle I|\text{Tr}D_{int}...$ provides the mean value of dipole moment. Initially, the system is in the ground state, and the bath is at equilibrium

$$|\rho(0)\rangle\rangle = |gg\rangle\rangle|\rho^{(eq)}\rangle$$

The dipole moment is independent of the bath variables so that $\mu^{(-)}$ is represented by the diagonal matrices in bath space

$$\hat{\mu}_1 = \begin{pmatrix} \mu_1 & 0 \\ 0 & \mu_1 \end{pmatrix} \qquad \hat{\mu}_2 = \begin{pmatrix} \mu_2 & 0 \\ 0 & \mu_2 \end{pmatrix}$$

In our basis set, $\mu^{(-)}$ is represented by the following matrices

$$\mu_{eg,gg}^{(-)} = \begin{pmatrix} \hat{\mu}_1 \\ \hat{\mu}_2 \end{pmatrix}$$

$$\mu_{ee,eg}^{(-)} = \begin{pmatrix} -\hat{\mu}_1 & 0 \\ -\hat{\mu}_2 & 0 \\ 0 & -\hat{\mu}_1 \\ 0 & -\hat{\mu}_2 \end{pmatrix}$$

$$\mu_{ee,ge}^{(-)} = \begin{pmatrix} \hat{\mu}_1 & 0 \\ 0 & \hat{\mu}_1 \\ \hat{\mu}_2 & 0 \\ 0 & \hat{\mu}_2 \end{pmatrix}$$

We further have $\mu_{ge,gg}^{(-)} = -\mu_{eg,gg}^{(-)}$, $\mu_{gg,eg}^{(-)} = [\mu_{eg,gg}^{(-)}]^T$, $\mu_{gg,ge}^{(-)} = [\mu_{ge,gg}^{(-)}]^T$, $\mu_{eg,ee}^{(-)} = [\mu_{ee,eg}^{(-)}]^T$, $\mu_{ee,ge}^{(-)} = [\mu_{ee,ee}^{(-)}]^T$. We note that $\mu_{\alpha,\beta} = [\mu_{\beta,\alpha}]^T$ and $\mu_{ij,kl}^{(-)} = -\mu_{ji,lk}^{(-)}$ for ij(kl) $\neq$ ee.

The linear response is given by

$$S(t_1) = i\langle I|\mu_{gg,eg}\mathcal{G}_{eg,eg}(t_1)\mu_{eg,gg}^{(-)}|\rho^{(eq)}\rangle + \text{c.c.}$$

In frequency space, $S(\omega_1) \equiv \int_0^\infty e^{i\omega_1 t_1}S(t_1)$. These represent a symmetric peak structure around ε and $-\varepsilon$, respectively, ($S(\omega)$

$= S^*(-\omega)$). We focus on the $\omega_1 \approx \varepsilon$ peaks. The absorption line shape is given by

$$I(\omega_1) = \text{Im } S(\omega_1) = \text{Re}\langle I|\mu_{gg,eg}\mathcal{G}_{eg,eg}(\omega_1)\mu_{eg,gg}^{(-)}|\rho^{(eq)}\rangle \quad (6)$$

We next turn to the third-order resonant signals generated in the $k_I = -k_1 + k_2 + k_3$ and $k_{II} = k_1 - k_2 + k_3$ phase-matching directions. These will be displayed as ω_1, ω_3 frequency–frequency plots $S(\omega_3,t_2,\omega_1)$ for various time slices t_2. As in the linear response (eq 6), each contribution to the third-order response has a complex conjugated counterpart giving peaks at opposite frequencies $S(\omega_3,t_2,\omega_1) = S^*(-\omega_3,t_2,-\omega_1)$.[27] We focus on the peak structure around $\omega_3 = \varepsilon$; the corresponding response function for the k_I signal is given by

$$S_I(\omega_3, t_2, \omega_1) = (i)^3[R_1(\omega_3, t_2, \omega_1) + R_2(\omega_3, t_2, \omega_1)]$$

and for k_{II}

$$S_{II}(\omega_3, t_2, \omega_1) = (i)^3[R_3(\omega_3, t_2, \omega_1) + R_4(\omega_3, t_2, \omega_1)] \quad (7)$$

The various contributions R (Liouville space pathways) are represented by the four Feynman diagrams shown in Figure 1

$$R_1(\omega_3, t_2, \omega_1) =$$
$$\langle I|\mu_{gg,eg}\mathcal{G}_{eg,eg}(\omega_3)\mu_{eg,gg}^{(-)}\mathcal{G}_{gg,gg}(t_2)\mu_{gg,ge}^{(-)}\mathcal{G}_{ge,ge}(\omega_1)\mu_{ge,gg}^{(-)}|\rho^{(eq)}\rangle$$

$$R_2(\omega_3, t_2, \omega_1) =$$
$$\langle I|\mu_{gg,eg}\mathcal{G}_{eg,eg}(\omega_3)\mu_{eg,ee}^{(-)}\mathcal{G}_{ee,ee}(t_2)\mu_{ee,ge}^{(-)}\mathcal{G}_{ge,ge}(\omega_1)\mu_{ge,gg}^{(-)}|\rho^{(eq)}\rangle$$

$$R_3(\omega_3, t_2, \omega_1) =$$
$$\langle I|\mu_{gg,eg}\mathcal{G}_{eg,eg}(\omega_3)\mu_{eg,gg}^{(-)}\mathcal{G}_{gg,gg}(t_2)\mu_{gg,eg}^{(-)}\mathcal{G}_{eg,eg}(\omega_1)\mu_{eg,gg}^{(-)}|\rho^{(eq)}\rangle$$

$$R_4(\omega_3, t_2, \omega_1) =$$
$$\langle I|\mu_{gg,eg}\mathcal{G}_{eg,eg}(\omega_3)\mu_{eg,ee}^{(-)}\mathcal{G}_{ee,ee}(t_2)\mu_{ee,eg}^{(-)}\mathcal{G}_{eg,eg}(\omega_1)\mu_{eg,gg}^{(-)}|\rho^{(eq)}\rangle \quad (8)$$

We shall further display the following combination of signals, which provide a clean absorptive signal[28]

$$S_A(\omega_3, t_2, \omega_1) \equiv -\text{Im } S_I(\omega_3, t_2, -\omega_1) - \text{Im } S_{II}(\omega_3, t_2, \omega_1) \quad (9)$$

4. Slow Fluctuations

The absorption spectrum (Figure 2) has four peaks, centered at two $E_{1(2),u} = (\varepsilon_{1u} + \varepsilon_{2u})/2 \pm (\Delta\varepsilon_u^2 + J_u^2)^{1/2}$ eigenvalues of H_u and two $E_{1(2),d} = (\varepsilon_{1d} + \varepsilon_{2d})/2 \pm (\Delta\varepsilon_d^2 + J_d^2)^{1/2}$ eigenvalues of H_d, in the static limiting case k_u, $k_d \ll |E_{1(2),u} - E_{1(2),d}|$

$$I(\omega) = \sum_{j=1}^2 \sum_{v=u;d} \frac{M_{j,v}^2\Gamma_v\rho_{ggv}^{(eq)}}{\Gamma_v^2 + (\omega - E_{j,v})^2} \quad (10)$$

where

$$M_{j,v} = \langle E_{j,v}|\mu|g\rangle$$

is the transition dipole and $\Gamma_d = k_u$ and $\Gamma_u = k_v$ are the line broadening parameters.

The 2D S_A line shape at short t_2, displayed in Figure 3, top left panel, shows primarily four diagonal peaks and four selected cross-peaks. Three consecutive interactions with laser pulses (applications of $\mu^{(-)}$) for times $t_2 \ll k_{d,u}^{-1}$ induce cross-peaks between peaks belonging to the same bath state but different excitons.

Coherent Multidimensional Spectroscopy of Excitons

J. Phys. Chem. B, Vol. 112, No. 45, 2008 **14215**

$$S_A(\omega_3, t_2 \ll k_{d,u}^{-1}, \omega_1) =$$

$$\text{Re} \sum_{k=1}^{2} \sum_{j=1}^{2} \sum_{v=u;d} M_{kv}^2 M_{jv}^2 \rho_{ggv}^{(eq)} \frac{1}{\Gamma_v - i(\omega_3 - E_{j,v})} \times$$

$$\left[\frac{2\Gamma_v}{\Gamma_v^2 + (\omega_1 - E_{k;v})^2} + e^{-\Gamma_{v,kj}^e t_2 - i(E_{j,v} - E_{k;v})t_2} \left(\frac{1}{\Gamma_v - i(\omega_1 - E_{j,v})} + \right. \right.$$

$$\left. \left. \frac{1}{\Gamma_v + i(\omega_1 - E_{k,v})} \right) \right] \quad (11)$$

where exciton dephasing $\Gamma_{v,kj}^e$ is negligible in the slow limit (compare fast fluctuation limit, section 5).

Additional cross-peaks induced by jumps among the u and d peaks (top left panel) appear for $t_2 \gg k_{d,u}^{-1}$. The dynamics is quite rich on these time scales since the phase relation between u and d eigenstates $\langle E_{j,u} | E_{i,d} \rangle$ is important for ee evolution and may also induce fluctuations of the peaks magnitudes at the $2\pi(E_{j,v} - E_{i;v})^{-1}$ period. We distinguish between two cases. If the u and d eigenstates are degenerate $|E_{j,u}\rangle = |E_{j,d}\rangle$, no exciton transport is allowed. This is shown in the top panels of Figure 3, where the delay time t_2 increases from the left to the right panel. The peaks gradually develop at all possible combinations of frequencies. However, peaks belonging to the same exciton are stronger even for very long times. When $|E_{j,u}\rangle \neq |E_{j,d}\rangle$, exciton transfer is allowed, and asymptotically, we have

$$\mathcal{G}_{\bar{E}_j \bar{E}_k v, \bar{E}_l \bar{E}_m w}(t_2 \to \infty) = \frac{1}{2} \delta_{jk} \delta_{lm} \frac{k_v}{k_u + k_d}$$

The absorptive line shape can then be factorized as follows

$$S_A(\omega_3, t_2 \to \infty, \omega_1) = 3 I(\omega_1) I(\omega_3) \quad (12)$$

This is similar to the asymptotic line shape of the monomer (eq 21).[29,30] Equation 12 holds for an arbitrary time scale and for any type of stochastic modulation (once transport is allowed). Equation 12 can be generalized beyond the stochastic model[31] to include finite temperature effects, where the emission line shape is red shifted with respect to the absorption (the Stokes shift).

Line shapes of these simple spectra are qualitatively reminiscent of 2D NMR spectra[33] measured on systems obeying similar dynamical rules. The general relation between 2D NMR methods and their optical counterpart has been discussed in ref

32. 2D NMR works on different time scales (with differences in models and approximations used) have no phase matching but have better control of the pulses. These differences and the rather weak fields applied in most optical experiments make the nonlinear response functions,[26] such as those used here, particularly adequate for interpreting 2D optical and infrared experiments.

For a more detailed analysis of these line shapes, we display the four contributions R_i to S_A in Figure 4. At $t_2 = 0$, $R_1 = R_2$ (Figure 4, top panels) since these diagrams only differ by the second interval evolution in the ee or gg manifolds. The ket and the bra action of the dipole moment connects different exciton states in t_1 and t_3 intervals, resulting in their cross-peaks. A similar peak pattern is seen in R_3, but this nonrephasing contribution is elongated in the antidiagonal direction compared to the diagonal elongation of the rephasing contribution. R_4 only shows diagonal peaks because the eg state in the third interval is caused by interaction with the first pulse and represents the same exciton state.

Figure 5 repeats these calculations in the long delay time regime $k_u t_2, k_d t_2 \gg 1$. The ground-state t_2 evolution for R_1 and R_3 mixes the u and d bath states, and their combination shows a complete peak structure. When the rephasing R_1 and non-rephasing R_3 contributions, characterized by the ground-state (gg) evolution during t_2, are summed over, the line shape may be recast as the product of the two line shapes, $\sim 2I(\omega_1)I(\omega_3)$.

The ee evolution in the R_2 and R_4 diagrams is more complex. During t_2, coherences decay, creating a statistical mixture of diagonal E_{jv} states. Since our parametrization does not allow exciton transport, we see decoherence. All contributions have different acting dipole moments at the first and second pulse decay. The only resulting cross-peaks are connected with the u and d jumps. This explains why the peaks are stronger in the S_A line shape. The features shown in Figure 5 are not universal. When exciton transport is allowed, the other cross-peaks appear, approaching eq 12.

The complete peak structure described above is simplified when the dipole moment does not couple to all of the $|E_{j,v}\rangle$ eigenstates or when some levels are accidently degenerate. The 2D line shapes can distinguish between various dynamical models with a similar absorption (1D) spectrum. To illustrate this, we compare the dimer with a two-state bath with the four-state jump bath model (FSJ) modulating a single chromophore,
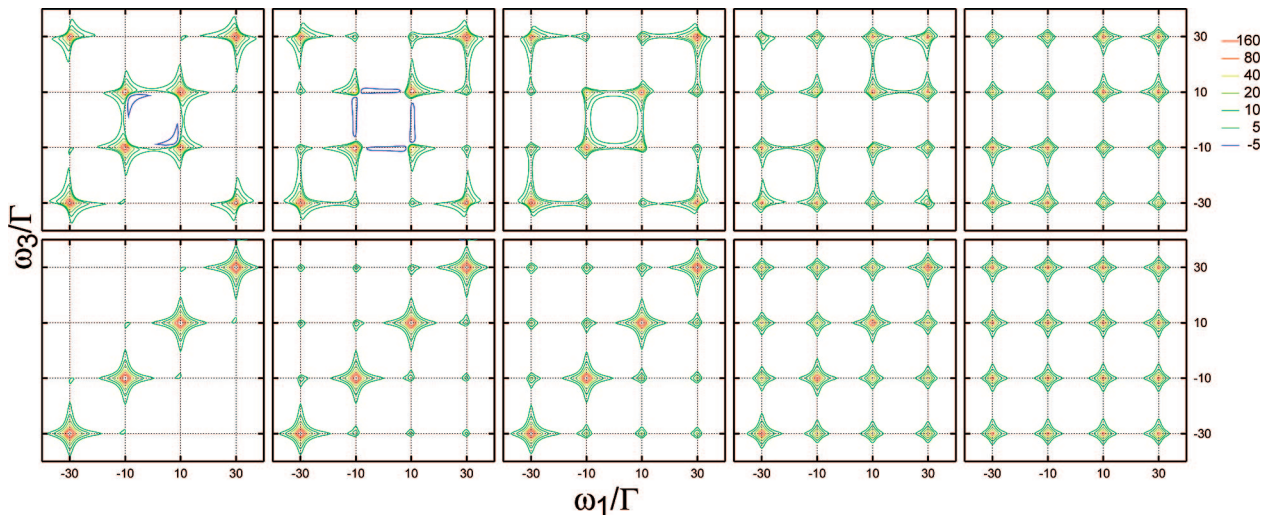

Figure 3. The S_A signal (eq 9) for a dimer with a two-state bath (top panels) and a monomer with a four-state bath (bottom panels) corresponding to Figure 2. For delay times $\Gamma t_2 = 0, 0.1, 0.2, 1.0, 100$ increasing from left to right. Other parameters are the same as those in Figure 2.
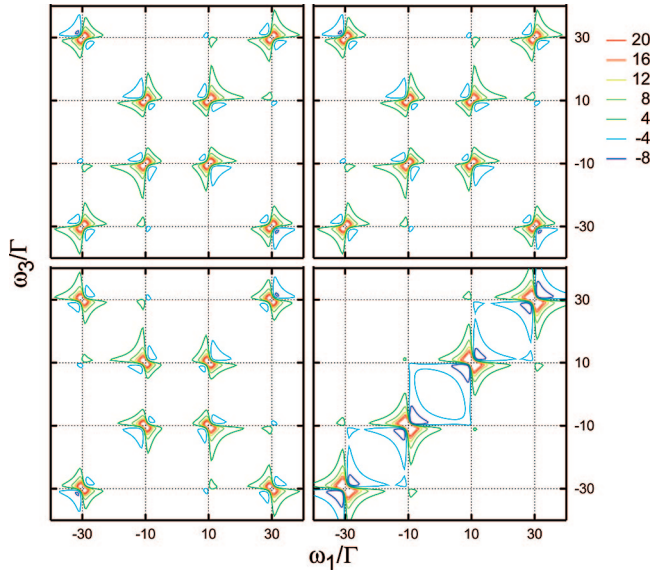
Figure 4. The $R_1(\omega_3,t_2,-\omega_1)$, $R_2(\omega_3,t_2,-\omega_1)$, $R_3(\omega_3,t_2,\omega_1)$, and $R_4(\omega_3,t_2,\omega_1)$ (eq 8, real parts) contributions to the S_A signal (from left to right, then top to bottom) for the dimer with a two-state bath for short delay times, $t_2 = 0$, corresponding to the most left top panel of Figure 2. Other parameters are the same as those in Figure 2.
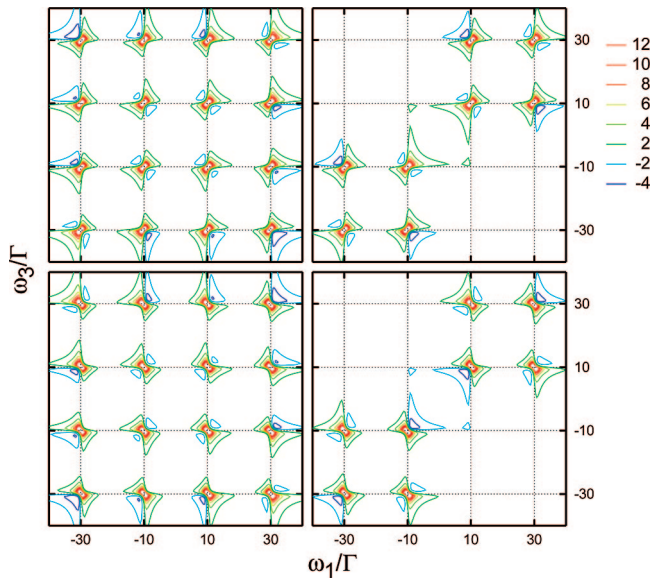

Figure 5. The same as in Figure 4 but for long delay times $\Gamma t_2 = 100$, corresponding to the most right top panel of Figure 3.

given in Appendix A. Comparison of eq 10 with eq 20 or the line shapes displayed in Figure 2 shows that the two models may have identical absorption line shapes in the static limit with the proper choice of the resonance frequencies and line width (as defined by eqs 10 and 20).

2D line shapes of the two models are markedly different at short times, as shown in Figure 3. The slow fluctuation FSJ limit (bottom left) S_A line shape at short t_2 jumps only reveals the diagonal peaks because no change of bath state can occur, in contrast to the dimer. With increasing delay time, the complete peak structure is developed; in contrast to the dimer, peak oscillations due to coherence dynamics (eq 11)[34] cannot be observed. Asymptotically, these two line shape agree (compare eqs 12, 21, and 22), except when exciton transfer is not allowed.
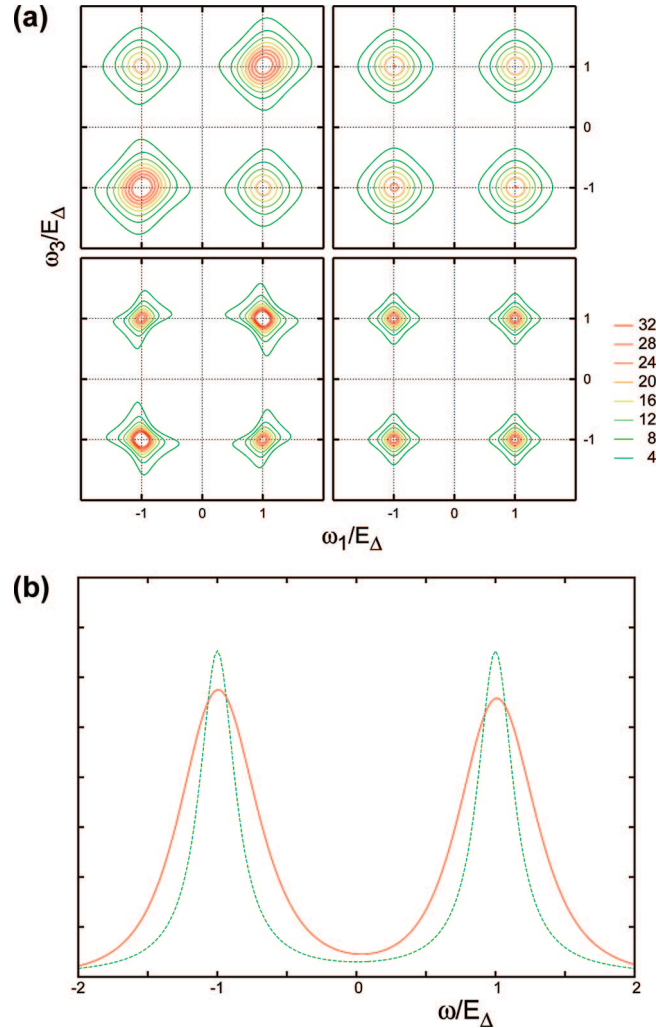

Figure 6. (A) Top: The S_A (eq 9) signal for the dimer with a two-state bath (eqs 3 and 4) for intermediate (top) and fast (bottom) fluctuations at short $t_2 = 0$ (left panels) and long $t_2 = 2000E_\Delta^{-1}$ (right panels) delay times. Measured in the peak splitting $E_\Delta \equiv [(\varepsilon_{1u} + \varepsilon_{1d})/4] - [(\varepsilon_{2u} + \varepsilon_{2d})/4]$. Parameters: Top: $\varepsilon_{1u} = 1.5E_\Delta$, $\varepsilon_{1d} = 0.5E_\Delta$, $\varepsilon_{2u} = -1.5E_\Delta$, $\varepsilon_{2d} = 0.5E_\Delta$, $J_u = -J_d = 0.68E_\Delta$, $k_u = k_d = k = 0.5E_\Delta$, $\mu_1 = \mu_2 = 1.189\,\mu$. Bottom: $\varepsilon_{1u} = 6.5E_\Delta$, $\varepsilon_{1d} = -0.45E_\Delta$, $\varepsilon_{2u} = -6.5E_\Delta$, $\varepsilon_{2d} = 4.5E_\Delta$, $J_u = -J_d = 0.75E_\Delta$, $k_u = k_d = k = 100E_\Delta$, $\mu_1 = \mu_2 = \mu$. (B) Absorption line shapes of the model of (A). The dashed line corresponds to fast limit (bottom of A), and the solid line corresponds to the intermediate limit (top of A).

5. Fast and Intermediate Fluctuations Time Scale

In the motional narrowing k_u, $k_d \gg |E_{ju} - E_{kd}|$ limit, fluctuations are averaged on the time scale of optical experiments. The averaged Hamiltonian

$$\bar{H} = \bar{\varepsilon}_1 B_1^\dagger B_1 + \bar{\varepsilon}_2 B_2^\dagger B_2 + \bar{J}(B_2^\dagger B_1 + B_1^\dagger B_2) \qquad (13)$$

where

$$\bar{J} = \frac{k_u J_u + k_d J_d}{k_u + k_d} \qquad \bar{\varepsilon}_j = \frac{k_u \varepsilon_{ju} + k_d \varepsilon_{jd}}{k_u + k_d}$$

may be used.

The dynamics is however different from the isolated dimer, which follows the Hamiltonian eq 13 since the fluctuations lead to an additional population relaxation rate (the exciton transfer) $\Gamma^T \sim \langle|\langle\bar{E}_1|(H - \bar{H})|\bar{E}_2\rangle|^2\rangle/k$ and dephasing rates $\Gamma^e \sim \Gamma^T + \sum_{i=1}^2 \langle\bar{E}_i|\langle(H - \bar{H})^2\rangle|\bar{E}_i\rangle/k$ and dephasing between ground and excited states $\Gamma_i \sim \Gamma^T/2 + \langle\bar{E}_i|\langle(H - \bar{H})^2\rangle|\bar{E}_i\rangle/k + \langle g|\langle(H - $

Coherent Multidimensional Spectroscopy of Excitons

J. Phys. Chem. B, Vol. 112, No. 45, 2008 **14217**

$\bar{H})^2)|g\rangle/k$. The averaged density matrix is approximately described by the Redfield master equations in the secular approximation in the high-temperature limit

$$\frac{d\rho_{\bar{E}_1\bar{E}_1}}{dt} = -\Gamma^{\mathrm{T}}\rho_{\bar{E}_1\bar{E}_1} + \Gamma^{\mathrm{T}}\rho_{\bar{E}_2\bar{E}_2}$$

$$\frac{d\rho_{\bar{E}_2\bar{E}_2}}{dt} = -\Gamma^{\mathrm{T}}\rho_{\bar{E}_2\bar{E}_2} + \Gamma^{\mathrm{T}}\rho_{\bar{E}_1\bar{E}_1}$$

$$\frac{d\rho_{\bar{E}_1\bar{E}_2}}{dt} = [-i(\bar{E}_1 - \bar{E}_2) - \Gamma^{\mathrm{e}}]\rho_{\bar{E}_1\bar{E}_2}$$

$$\frac{d\rho_{\bar{E}_jg}}{dt} = [-i\bar{E}_j - \Gamma_j]\rho_{\bar{E}_jg}$$

The dynamics may be described in the reduced system Liouville space. Signatures of the fluctuations are present in the relaxation and dephasing rates, which may not be described in the Hilbert space. The corresponding Green's functions in system Liouville space are

$$\mathscr{G}_{\bar{E}_1\bar{E}_1,\bar{E}_1\bar{E}_1}(t) = \mathscr{G}_{\bar{E}_2\bar{E}_2,\bar{E}_2\bar{E}_2}(t) = \frac{1 + e^{-2\Gamma^{\mathrm{T}}t}}{2}$$

$$\mathscr{G}_{\bar{E}_1\bar{E}_1,\bar{E}_2\bar{E}_2}(t) = \mathscr{G}_{\bar{E}_2\bar{E}_2,\bar{E}_1\bar{E}_1}(t) = \frac{1 - e^{-2\Gamma^{\mathrm{T}}t}}{2}$$

$$\mathscr{G}_{\bar{E}_1\bar{E}_2,\bar{E}_1\bar{E}_2}(t) = \mathscr{G}_{\bar{E}_2\bar{E}_1,\bar{E}_2\bar{E}_1}^*(t) = e^{[-i(\bar{E}_1-\bar{E}_2)-\Gamma^{\mathrm{e}}]t}$$

$$\mathscr{G}_{\bar{E}_jg,\bar{E}_jg}(t) = \mathscr{G}_{g\bar{E}_j,g\bar{E}_j}^*(t) = e^{[-i\bar{E}_j - \Gamma_j]t}$$

Note that the SLE provides an exact representation of stochastic Markovian fluctuations of Hamiltonian dynamics. Both the Liouville equation and the averaging over bath paths preserve the positive semidefiniteness of the density matrix; so does the SLE. The positivity issue of master equations,[35] which is a major problem for the Redfield equations when the secular approximation is not invoked, is avoided.

The absorption spectrum has two peaks centered at the eigenvalues $\bar{E}_1$ and $\bar{E}_2$ of the averaged dimer Hamiltonian

$$I(\omega) = \sum_{i=1}^{2} \frac{M_i^2 \Gamma_i}{(\Gamma_i)^2 + (\omega - \bar{E}_i)^2}$$

If $\Gamma_1 + \Gamma_2 > \bar{E}_1 - \bar{E}_2$, these can eventually overlap and merge into a single peak. The 2D line shape (Figure 6, bottom line) has two cross-peaks induced by the annihilation of one excitation by the second pulse and the creation of different excitation by the third pulse also for short t_2.

$$S_{\mathrm{A}}(\omega_3, t_2, \omega_1) =$$

$$\sum_{i=1}^{2}\sum_{j=1}^{2} 2M_i^2 M_j^2 \frac{\Gamma_i}{(\Gamma_i)^2 + (\omega_1 - \bar{E}_i)^2} \frac{\Gamma_j}{(\Gamma_j)^2 + (\omega_3 - \bar{E}_j)^2} +$$

$$\mathrm{Re}\sum_{i,j,k,l=1}^{2} \frac{M_iM_jM_kM_l\mathscr{G}_{\bar{E}_i\bar{E}_k,\bar{E}_j\bar{E}_i}(t_2)}{\Gamma_l - i(\omega_3 - \bar{E}_l)} \times$$

$$\left[\frac{1}{\Gamma_j - i(\omega_1 - \bar{E}_j)} + \frac{1}{\Gamma_i + i(\omega_1 - \bar{E}_i)}\right]$$

This is different from two-state jump model line shapes in the slow modulation limit.[20] The cross-peaks have intensities comparable with the diagonal peaks at long times.
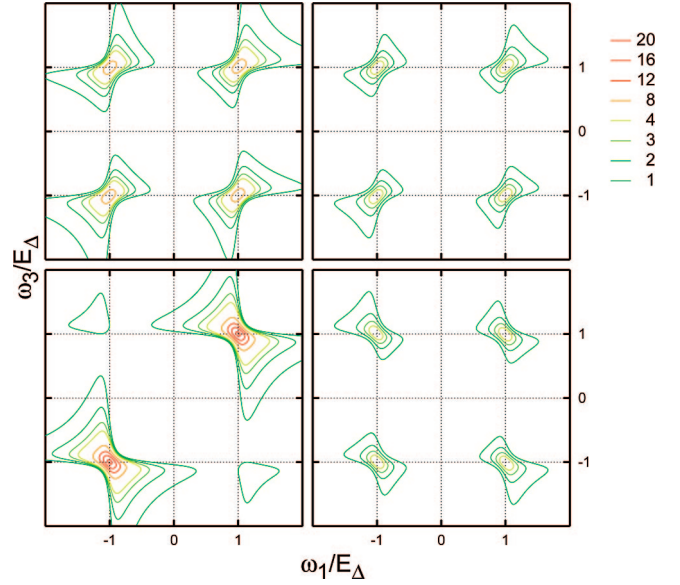
Figure 7. The R_3 (top panel) and R_4 (bottom panel) signal (eq 8, real parts) for the dimer in the fast modulation limit for short $t_2 = 0$ (left panels) and long $t_2 = 2000E_\Delta^{-1}$ (right panels) delay times. Other parameters are as those in Figure 6A, bottom.
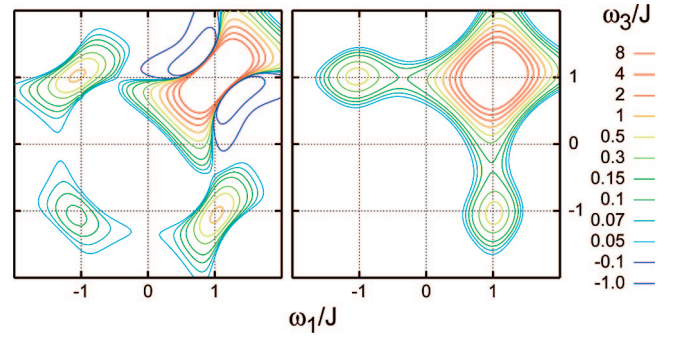
Figure 8. The S_{A} line shape of a dimer with spectral diffusion for short $\Lambda t_2 = 0$ (left panel) and long $\Lambda t_2 = 2$ (right panel) times. Other parameters: $\mu_1 = \mu_2 = 1$, $J_u = J_d = J$, $f(Q) = Q$, $\sigma_1 = \sigma_2 = 0.3J$, $\Lambda_1 = \Lambda_2 = \Lambda = 0.1J$, $\varepsilon_{1d} = \varepsilon_{1u} = \varepsilon_{1d} = \varepsilon_{1u} = 0.0$.

The limiting cases of slow or fast fluctuations can be treated by a simpler methods; the stochastic approach is however essential for the intermediate regime.

Figure 6 compares the intermediate (top) and fast (bottom) fluctuation limit. The separated peaks of the static case overlap and merge into a single peak. In the intermediate regime, however, the memory of the two-bath states can still be tracked by the diagonal elongation of peaks at short times. In the fast limit, the peaks become narrower, and all signatures of memory are erased. Panel B shows the corresponding absorption line shapes.

At longer delay times (right panels), the decoherence and exciton transport erase all memory, and line shapes approach eq 12. The t_2 dependence follows from the ee t_2 evolution of R_2 and R_4, while the R_1 and R_3 contributions give half of the product (eq 21) (not shown).

The intermediate time scale shows additional delicate effects caused by altering the eigenvectors (rather then merely eigenvalues) of the Hamiltonian. These will be discussed in the next section using a Gaussian model for spectral diffusion.

We next examine more closely the R_3 and R_4 contributions (Figure 7). At short times $\mathscr{G}_{\bar{E}_i\bar{E}_k,\bar{E}_j\bar{E}_i} = \delta_{lj}\delta_{ik}$, and R_3 follows the four peak structure identical to R_1, while R_4 is diagonal, for the

same reason as that mentioned in Figure 4. At long times, t_2 coherences are dumped. Asymptotically, $\mathcal{G}_{\bar{E}_l\bar{E}_k,\bar{E}_j\bar{E}_i} = 1/2\delta_{lk}\delta_{ij}$, and the line shape (eq 12) is restored. This argument holds as long as exciton transfer is allowed, $\delta J \neq 0$; otherwise, the picture of Figure 5 is repeated. and the cross-peaks never show up in R_4.

6. Spectral Diffusion

We now turn to a different model representing the coupling to uncorrelated continuous diagonal frequency fluctuations. This situation, very common in molecular aggregates, is described by adding the following coupling term

$$H_{SQ} = f_1(Q_1(t))B_1^\dagger B_1 + f_2(Q_2(t))B_2^\dagger B_2$$

to the Hamiltonian, together with a Fokker−Planck master equation for the density evolution of the two collective coordinates Q_1 and Q_2

$$\left(\frac{\partial\rho(Q_1,Q_2)}{\partial t}\right)_Q = \sum_{w=1}^{2}\Lambda_w\frac{\partial}{\partial Q_w}\left(Q_w + \sigma_w^2\frac{\partial}{\partial Q_w}\right)\rho(Q_1,Q_2) = \mathcal{L}^Q\rho \tag{14}$$

This model assumes that bath motions primarily alter (and in simple way) the local site frequencies. The resulting delocalized eigenenergy changes are secondary and more complicated. Standard simulations of aggregates rely on diagonalization of the averaged Hamiltonian, allowing an arbitrary time scale for Gaussian diagonal fluctuations (diagonal in the eigenbasis) but only fast (if any) fluctuations for the off-diagonal. This make the problem numerically tractable, however, it may not always hold. Our aim here is to treat arbitrary time scales for off-diagonal (in eigenbasis) fluctuations by using the SLE and to show significant differences from the more approximate treatments. This may lead to the development of better approximations that retain the reduced bath treatment (necessary for large aggregates) but properly includes effects of the bath time scale. For smaller aggregates, the SLE can be directly used to calculate 2D spectra.

The SLE assumes the form

$$\frac{d\rho}{dt} = -i[H + H_{SQ}, \rho] + \left(\frac{d\rho}{dt}\right)_M + \left(\frac{d\rho}{dt}\right)_Q$$

The eigenvectors of the Fokker−Planck operator eq 14 are direct products of two single Fokker−Planck variables Q_1, Q_2

$$\phi_{\alpha\beta} = \phi_\alpha^1\phi_\beta^2 \tag{15}$$

The eigenvectors are given by

$$\phi_\alpha^w = \frac{\exp[-(Q_w/\sigma_w)^2]}{2^\alpha\sqrt{2\pi}\alpha!\,\sigma_w}\mathcal{H}_\alpha\left(\frac{Q_w}{\sigma_w\sqrt{2}}\right)$$

where $\mathcal{H}_\alpha$ are Hermite polynomials

$$\mathcal{H}_\alpha(x) = (-1)^\alpha e^{x^2}\frac{d^\alpha}{dx^\alpha}e^{-x^2}$$

where $\{\phi_{\alpha\beta}\}$, $\alpha = 0, 1, 2,...$ and $\beta = 0, 1, 2,...$, correspond to eigenvalues $-\alpha\Lambda_1 - \beta\Lambda_2$ and form the suitable basis for a matrix representation of bath densities.[36] The matrix elements of $\mathcal{L}^Q$ are

$$[\mathcal{L}^Q]_{\alpha\beta,\gamma\eta} = (-\alpha\Lambda_1 - \beta\Lambda_2)\delta_{\alpha,\gamma}\delta_{\beta,\eta} \tag{16}$$

The Q variable is represented by the following matrix

$$[Q_1]_{\alpha\beta,\gamma\eta} = \left(\alpha\sigma_1\sqrt{2}\delta_{\alpha-1,\gamma} + \frac{\sigma_1}{\sqrt{2}}\delta_{\alpha,\gamma-1}\right)\delta_{\beta\eta}$$

$$[Q_2]_{\alpha\beta,\gamma\eta} = \left(\beta\sigma_2\sqrt{2}\delta_{\beta-1,\eta} + \frac{\sigma_2}{\sqrt{2}}\delta_{\beta,\eta-1}\right)\delta_{\alpha\gamma} \tag{17}$$

If H_{SQ} is a polynomial in Q_1 and Q_2, it can be represented by the block-tridiagonal matrix, and the algorithm of refs 10, 20, and 36 may be employed to obtain the Green's function by inverting the block-tridiagonal matrices (eq 5). For instance, the linear coupling $c_1Q_1 + c_2Q_2 + c_{12}Q_1Q_2$ becomes tridiagonal in blocks $\{\phi_{00}\}$, $\{\phi_{10}, \phi_{11}, \phi_{01}\}$, $\{\phi_{20}, \phi_{21}, \phi_{22}, \phi_{12}, \phi_{02}\},...$ However, the SLE approach is not limited to any particular form of the coupling; f can be an arbitrary function.

The zero eigenvector $\rho^{Q;(eq)} = \phi_{00}$ (or in the matrix notation $[\rho^{eq}]_{\alpha\beta} = \delta_{\alpha0}\delta_{\beta0}$) gives the equilibrium distribution. Summation over the bath $\int dQ_1 dQ_2$ corresponds to zero left eigenvector in the eigenbasis $\{\phi_\alpha\}$; thus, $\langle I^Q|_{\alpha\beta} = \delta_{\alpha0}\delta_{\beta0}$. The initial state is a direct product of equilibrium densities of all of the bath variables $|\rho^{(eq)}\rangle|\rho^{Q;(eq)}\rangle$ and, similarly, the final summation.

The various Liouville space exciton manifold blocks of the Liouville superoperator $\mathcal{L}^{SQ} = -i[H_{SQ},...]$ are

$$\mathcal{L}_{gg,gg}^{SQ} = 0$$

$$\mathcal{L}_{eg,eg}^{SQ} = \begin{pmatrix} -if_1(Q_1) & 0 & 0 & 0 \\ 0 & -if_1(Q_1) & 0 & 0 \\ 0 & 0 & -if_2(Q_2) & 0 \\ 0 & 0 & 0 & -if_2(Q_2) \end{pmatrix}$$

$$\mathcal{L}_{ee',ee'}^{SQ} = $$

$$\begin{pmatrix} 0 & 0 & 0 & 0 & 0 & 0 & 0 & 0 \\ 0 & 0 & 0 & 0 & 0 & 0 & 0 & 0 \\ 0 & 0 & -i(f_1-f_2) & 0 & 0 & 0 & 0 & 0 \\ 0 & 0 & 0 & -i(f_1-f_2) & 0 & 0 & 0 & 0 \\ 0 & 0 & 0 & 0 & i(f_1-f_2) & 0 & 0 & 0 \\ 0 & 0 & 0 & 0 & 0 & i(f_1-f_2) & 0 & 0 \\ 0 & 0 & 0 & 0 & 0 & 0 & 0 & 0 \\ 0 & 0 & 0 & 0 & 0 & 0 & 0 & 0 \end{pmatrix}$$

Here $f_1 \equiv f_1(Q_1)$ and $f_2 \equiv f_2(Q_2)$. The response can still be calculated using (eq 8) but now in the higher space, which combines Q with the u, d space.

Several methods have been employed to describe the signatures of spectral diffusion in the nonlinear response of aggregates. Standard simulations use the Redfield equations for the evolution of the exciton density matrix during t_2, and a Gaussian peak of an arbitrary relaxation time scale for peaks can be added.[1] Static disorder in site frequencies can be easily incorporated. Slow fluctuations only account for peak shape, interlevel coupling fluctuation are fast, and dynamical effects on dipole moments are neglected.

The SLE framework is more general. Consider a symmetric dimer $J_u = J_d$, $\varepsilon_1 = \varepsilon_2$, $\mu_1 = \mu_2$, where only the symmetric eigenvector $|E_1\rangle = |1\rangle + |2\rangle$ is radiatively coupled to the ground state. For fast spectral diffusion, the other peak $|E_2\rangle = |1\rangle - |2\rangle$ is dark. However, when the slow coordinate nonequilibrium eigenstates $|E_2(Q_1, Q_2)\rangle$ couple to the dipole moment $\langle E_2(Q_1, Q_2)|\mu|g\rangle \neq 0$, the other peak may be observed (Figure 8, left panel). The SLE can consistently describe the fluctuation time scales where the additional diagonal peak vanishes (Figure 8, right panel). This is not properly described by simulations at the Redfield level, which do not account for the necessary correlations between Liouville space and bath coordinates during
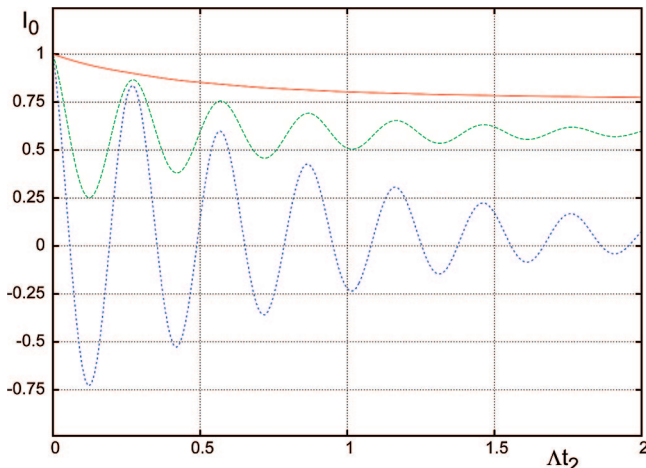
Coherent Multidimensional Spectroscopy of Excitons

J. Phys. Chem. B, Vol. 112, No. 45, 2008 **14219**

Figure 9. The relative intensities of peaks (against t_2 value) at the $I_0(t_2) = S_A(\omega_3, t_2, \omega_1)/S_A(\omega_3, 0, \omega_1)$ line shape of a dimer with spectral diffusion for varying delay times t_2 at the diagonal peak $\omega_1 = \omega_3 = J$ (solid line), the cross-peak at $\omega_1 = -\omega_3 = J$ (dashed line), and the transitory diagonal $\omega_1 = \omega_3 = -J$ (dotted line). Other parameters are as those in Figure 8.

the transport. Additional static disorder can induce some oscillator strength to the dark state but cannot describe its evolution.

At zero delay time, the magnitude of the $(-1,-1)$ peak is proportional to the probability $\tilde{p}$ that bath coordinates shift the site energies ε so that the dipole moment $\langle E_2(Q_1, Q_2)|\mu|g\rangle$ is substantial. Such configurations are rather rare and far from equilibrium; therefore, they disappear at relaxation time scale Λ^{-1}. For $t_2 \gg \Lambda^{-1}$, the $(-1,-1)$ peak can only be induced by two independent hits of the "$\tilde{p}$" area; therefore, its magnitude is quadratically proportional to $\tilde{p}$, in agreement with asymptotic formula eq 12.

These effects are illustrated in Figure 9, which depicts the magnitudes (normalized with respect to $t_2 = 0$) of all peaks in Figure 8 as they vary with the delay time t_2. We see significant decay of the $(-1,-1)$ peak at the Λ^{-1} time scale, as discussed. The $(1,1)$ diagonal and the cross-peak $(1,-1)$ (the other cross-peak $(-1,1)$ has the same magnitude) change less significantly because the cross-peak requires an instantaneous dipole moment for the dark state only in the t_1 (peak $(1,-1)$) or t_3 intervals (peak $(-1,1)$). Its magnitude thus remains linear in p (for small p) for any delay times. In addition, we see oscillation of the peaks caused by the coherent dynamics, as predicted by the Redfield level of theory[34,37] and observed experimentally.[38] Such oscillations require the interplay of both exciton states. The effect is thus most pronounced for $(-1,-1)$ and the cross-peak and not for the $(1,1)$ peak.

7. Conclusions

It is straightforward to extend the present model to other types of excitonic systems as long as the fluctuations are Markovian. In fact, the code developed for the present calculations can treat any number of ground, excited, and doubly excited states and multistate or Gaussian–Markovian fluctuations (coordinate linearly or quadratically coupled to the Q coordinate). Since the computational time grows exponentially with the number of stochastic coordinates, applications to extended excitonic systems will require the identification of a few relevant coordinates.

We showed that the SLE approach is an essential tool for describing the intermediate time scale of fluctuations and may

thus be used to test various approximate methods[39,40] developed in order to avoid the numerically expensive explicit representation of the stochastic coordinate.

The SLE assume that the stochastic process is independent of the state of the system. This is justified at high temperatures. Finite-temperature effects such as the Stokes shift or nonuniform exciton distributions are missed. The Redfield equations, in contrast, contain finite-temperature effects. The high-temperature $\hbar\Delta\varepsilon < kT$ limit usually holds for the infrared[19,21] but not in the optical domain at room temperature. Finite-temperature corrections for linear coupling include system-dependent bath dynamics.[16,41–44] Provided that the temperature is not too low, the equations of motion have the same complexity as the SLE and may be readily implemented, if necessary. This level was widely used to describe electron-transfer processes (adiabatic and nonadiabatic). At very low temperatures, when the quantization of bath degrees of freedom is necessary, some additional oscillator modes with Matsubara frequencies have to be added, increasing computation costs.[16]

Appendix A. The Four-State Jump (FSJ) Model

We consider a single two-level chromophore described by the Hamiltonian

$$H = \varepsilon(t)B^\dagger B \tag{18}$$

where ε_s assumes four possible values, $s = 1, 2, 3, 4$. The model has a four-peak linear spectrum indistinguishable from the TSJ dimer (Figure 2). This model has 12 rates k_{sr} for the transitions between r and s states. The time evolution is described by the master equation

$$\frac{d\rho_s}{dt} = -\sum_{r \neq s} k_{rs}\rho_s + \sum_{r \neq s} k_{sr}\rho_r \tag{19}$$

Equation 19 further describes the evolution in the gg and ee manifolds because no coherence is connected with the ground (excited)-state evolution.

The SLE for the coherence evolution is

$$\frac{d\rho_{egs}}{dt} = -i\varepsilon_s\rho_{egs} - \sum_{r \neq s} k_{rs}\rho_{egs} + \sum_{r \neq s} k_{sr}\rho_{egr}$$

The rates were chosen to yield the same linear spectrum as the TSJ dimer in the slow limit

$$I(\omega) = \mu^2 \sum_{v=1}^{4} \frac{\Gamma_v \rho_{ggv}^{(eq)}}{[\Gamma_v^2 + (\omega_1 - \varepsilon_v)^2]} \tag{20}$$

with $\Gamma_v = \sum_{r \neq v} k_{rv}$.

Consider the 2D line shape in the slow jumps limit $k_{rs}/(\varepsilon_r - \varepsilon_s) \ll 1$. At short times, $k_{rs}t_2 \ll 1$ line shapes show only diagonal peaks at fundamental frequencies. Cross-peaks are absent (Figure 3 bottom left panel)

$$S_A(\omega_3, t_2 = 0, \omega_1) = \mu^4 \sum_{v=1}^{4} \frac{\Gamma_v^2 \rho_{ggv}^{(eq)}}{[\Gamma_v^2 + (\omega_1 - \varepsilon_v)^2][\Gamma_v^2 + (\omega_3 - \varepsilon_v)^2]}$$

Since there is no coherence during t_2, the S_A line shape will only change at the k^{-1} time scale, where the cross-peaks appear. Asymptotically, the line shape approaches the factorized form

$$S_A(\omega_3, t_2 \to \infty, \omega_1) = 4I(\omega_1)I(\omega_3) \qquad (21)$$

This limit holds for all one-exciton stochastic line shapes with finite memory; see ref 30 for some exceptions when the memory persists for arbitrary time scales. A similar relation can be generalized for the first manifold contribution of any excitonic system, which allows the excitonic transfer toward the thermodynamic high-temperature uniform excitonic distribution

$$S_A(\omega_3, t_2 \to \infty, \omega_1) = 2\frac{n+1}{n}I(\omega_1)I(\omega_3) \qquad (22)$$

where n is the number of excitons.[31]

References and Notes

(1) Abramavicius, D.; Mukamel, S. *Chem. Rev.* **2004**, *104*, 2073.

(2) Woutersen, S.; Hamm, P. *J. Phys.: Condens. Matter* **2002**, *14*, R1035.

(3) Meinhold, L.; Smith, J. C.; Kitao, A.; Zewail, A. H. *Proc. Natl. Acad. Sci. U.S.A.* **2007**, *104*, 17261.

(4) Nilsson, L.; Halle, B. *Proc. Natl. Acad. Sci. U.S.A.* **2005**, *102*, 13867.

(5) Lim, M.; Hamm, P.; Hochstrasser, R. M. *Proc. Natl. Acad. Sci. U.S.A.* **1998**, *95*, 15315.

(6) Ganim, Z.; Tokmakoff, A. *Biophys. J.* **2006**, *91*, 2636.

(7) Cowan, M. L.; Bruner, B. D.; Huse, N.; Dwyer, J. R.; Chugh, B.; Nibbering, E. T. J.; Elsaesser, T.; Miller, R. J. D. *Nature* **2005**, *434*, 199.

(8) Brixner, T.; Stenger, J.; Vaswani, H. M.; Cho, M.; Blankenship, R. E.; Fleming, G. R. *Nature* **2005**, *434*, 625.

(9) Jansen, T. L. C.; Knoester, J. *J. Chem. Phys.* **2007**, *127*, 234502.

(10) Jansen, T. L. C.; Zhuang, W.; Mukamel, S. *J. Chem. Phys.* **2004**, *121*, 10577.

(11) Abramavicius, D.; Zhuang, W.; Mukamel, S. *J. Phys. Chem. B* **2004**, *108*, 18034.

(12) Redfield, A. G. *Adv. Magn. Reson.* **1965**, *1*, 1.

(13) May V.; Kuhn, O. *Charge and Energy Transfer Dynamics in Molecular Systems*; Wiley-VCH: Weinheim, Germany, 1999.

(14) Szöcz, V.; Palszegi, T.; Lukeš, V.; Sperling, J.; Milota, F.; Jakubetz, W.; Kauffmann, H. F. *J. Chem. Phys.* **2006**, *124*, 124511.

(15) Kubo, R. *J. Math. Phys.* **1963**, *4*, 174.

(16) Tanimura, Y. *J. Phys. Soc. Jpn.* **2006**, *75*, 082001.

(17) Gamliel, D.; Levanon H. *Stochastic Processes in Magnetic Resonance*; World Scientific: River Edge, NJ, 1995.

(18) Jansen, T. L. C.; Hayashi, T.; Zhuang, W.; Mukamel, S. *J. Chem. Phys.* **2005**, *123*, 114504.

(19) Kim, Y. S.; Hochstrasser, R. M. *Proc. Natl. Acad. Sci. U.S.A.* **2005**, *102*, 1185.

(20) Šanda, F.; Mukamel, S. *J. Chem. Phys.* **2006**, *125*, 014507.

(21) Zheng, J.; Kwak, K.; Asbury, J.; Chen, X.; Piletic, I. R.; Fayer, M. D. *Science* **2005**, *309*, 1338.

(22) Davydov, A. S. *Theory of Molecular Excitons*; McGraw-Hill: New York, 1962.

(23) Silinsh, E. A., Čápek, V. *Organic Molecular Crystals: Interaction, Localization and Transport Phenomena*; AIP Press: New York, 1994.

(24) van Amerogen, H.; Valkunas, L.; van Grondelle, R. *Photosyntetic Excitons*; World Scientific: Singapore, 2000.

(25) van Kampen, N. G. *Stochastic Processes in Physics and Chemistry*; North Holland: Amsterdam, The Netherlands, 1992.

(26) Mukamel, S. *Principles of Nonlinear Optical Spectroscopy*, Oxford University Press: New York, 1995.

(27) Jonas, D. M. *Annu. Rev. Phys. Chem.* **2003**, *54*, 425.

(28) Khalil, M.; Demirdöven, N.; Tokmakoff, A. *Phys. Rev. Lett.* **2003**, *90*, 047401.

(29) Šanda, F.; Mukamel, S. *Phys. Rev. Lett.* **2007**, *98*, 080603.

(30) Šanda, F.; Mukamel, S. *J. Chem. Phys.* **2007**, *127*, 154107.

(31) As noted in ref 30, for a single chromophore, eq 22 may be generalized beyond the stochastic model. For a multiexcitonic but exciton-conserving Hamiltonian, the four diagrams of Figure 1 contribute $\hbar S_A(\omega_3, t_2 = \infty, \omega_1) = I(\omega_1)[I(\omega_3) + I_E(\omega_3)]$, where I_E is the emission line shape obtained from the excited-state equilibrium ρ_ν, assuming the asymptotic Green's function (of gg and ee manifold) approach $[G]_{\nu\nu'}(t \to \infty) = \rho_\nu \text{Tr}_{\nu'}$ in some suitable representation, where ν is a multiindex (quantum or classical) completely describing the excited (ground) state of the system. Additional contribution to S_A could, however, come from the excited-state absorption (involving the second exciton manifold).

(32) Scheurer, Ch.; Mukamel, S. *J. Chem. Phys.* **2001**, *115*, 4989.

(33) Ernst, R. R.; Bodenhausen, G.; Wokaun, A. *Principles of Nuclear Magnetic Resonance in One and Two Dimensions*; Oxford University Press: New York, 1987.

(34) Pisliakov, A. V.; Mančal, T.; Fleming, G. R. *J. Chem. Phys.* **2006**, *124*, 234505.

(35) Alicki, R.; Lendi, K. *Quantum Dynamical Semigroups and Applications*; Springer: Berlin, Germany, 1987.

(36) Risken H. *The Fokker–Plank Equation*; Springer: Berlin, Germany, 1989.

(37) Kjellberg, P.; Brüggemann, B.; Pullerits, T. *Phys. Rev. B* **2006**, *74*, 024303.

(38) Engel, G. S.; Calhoun, T. R.; Read, E. L.; Ahn, T. K.; Mančal, T.; Cheng, Y.-C.; Blankenship, R. E.; Fleming, G. R. *Nature* **2007**, *446*, 782.

(39) Kim, H. D.; Tanimura, Y.; Cho, M. *J. Chem. Phys.* **2007**, *127*, 075101.

(40) Abramavicius, D.; Valkunas, L.; Mukamel, S. *Europhys. Lett.* **2007**, *80*, 17005.

(41) Garg, A.; Onuchic, J. N.; Ambegaokar, V. *J. Chem. Phys.* **1985**, *83*, 4491.

(42) Zusman, D. *Chem. Phys.* **1980**, *49*, 295.

(43) Chernyak, V.; Mukamel, S. *J. Chem. Phys.* **1996**, *105*, 4565.

(44) Ishizaki, A.; Tanimura, Y. *J. Chem. Phys.* **2006**, *125*, 084501.